

Adaptive confidence thresholding for monocular depth estimation

Hyesong Choi^{1*}, Hunsang Lee^{2*}, Sunkyung Kim¹, Sunok Kim³,
Seungryong Kim⁴, Kwanghoon Sohn², Dongbo Min^{1†}

¹Ewha W. University, ²Yonsei University, ³Korea Aerospace University, ⁴Korea University

Abstract

Self-supervised monocular depth estimation has become an appealing solution to the lack of ground truth labels, but its reconstruction loss often produces over-smoothed results across object boundaries and is incapable of handling occlusion explicitly. In this paper, we propose a new approach to leverage pseudo ground truth depth maps of stereo images generated from self-supervised stereo matching methods. The confidence map of the pseudo ground truth depth map is estimated to mitigate performance degeneration by inaccurate pseudo depth maps. To cope with the prediction error of the confidence map itself, we also leverage the threshold network that learns the threshold dynamically conditioned on the pseudo depth maps. The pseudo depth labels filtered out by the thresholded confidence map are used to supervise the monocular depth network. Furthermore, we propose the probabilistic framework that refines the monocular depth map with the help of its uncertainty map through the pixel-adaptive convolution (PAC) layer. Experimental results demonstrate superior performance to state-of-the-art monocular depth estimation methods. Lastly, we exhibit that the proposed threshold learning can also be used to improve the performance of existing confidence estimation approaches.

1. Introduction

Monocular depth estimation, which predicts a dense depth map from a single image, plays an important role in various fields such as scene understanding and autonomous driving. Early works [7, 30, 3] are based on supervised learning in which the performance depends on a huge amount of training data with ground truth depth labels.

This work was supported by the Institute of Information & Communications Technology Planning & Evaluation (IITP) grant funded by the Korean government (MSIT) (No. 2020-0-00056) and the Mid-Career Researcher Program through the NRF of Korea (NRF-2021R1A2C2011624). S. Kim⁴ was supported in part by the MSIT under the ICT Creative Consilience Program (IITP-2021-2020-0-01819).

* Equal contribution. † Corresponding author: dbmin@ewha.ac.kr

Since establishing such a large-scale training data is very costly and labour-intensive, recent approaches rely on the self-supervised learning regime [10, 12, 31, 13, 35]. Instead of using ground truth labels for training the network, they attempt to leverage the self-supervision from a pair of stereo images or monocular video sequences, under the assumption that the geometric structure of a scene can be encoded with the reconstruction loss based on pixel-wise intensity similarities [10]. This loss function seems to be an appealing alternative to the lack of large-scale ground truth labels, but it often leads to blurry results around depth boundaries and does not consider occluded pixels [12].

Instead of relying on the self-supervised reconstruction loss across stereo images, Cho *et al.* [5] attempted to train the monocular depth estimation network through *pseudo* depth labels of the stereo images generated from pre-trained stereo matching network [33]. To mitigate performance degeneration by inaccurate pseudo depth labels, they leverage stereo confidence maps ($\in [0, 1]$) indicating the reliability of the pseudo depth labels. The confidence map is truncated with a threshold [5, 45] so that depth values with low confidence are excluded. However, a fixed threshold for all training dataset still has the risk of inaccurate pseudo depth values being used in the network training [5]. The method of [45] attempted to address this issue by learning the threshold with an additional regularization term, but the performance gain is rather limited due to its hard thresholding and the implicit constraint by the regularization term.

To overcome this limitation, we propose a novel architecture that adaptively learns the threshold dynamically conditioned on the pseudo depth map. For a given inaccurate pseudo depth map, the stereo confidence map and its associated threshold are inferred in an end-to-end manner. The confidence map is then thresholded through a differential soft-thresholding operator controlled by the learned threshold. The proposed threshold learning is capable of dealing with the prediction errors of the confidence map more effectively. Note that we leverage the soft-thresholding operator to make the network differentiable. The thresholded confidence map is then used together with

the pseudo depth labels for training the monocular depth estimation network. Additionally, we propose to enhance the monocular depth map in a probabilistic inference framework. Unreliable parts of the monocular depth map are identified using the uncertainty map, and these are refined through the pixel-adaptive convolution (PAC) layer [44]. Experimental results validate that the monocular depth accuracy is significantly improved by leveraging the proposed threshold learning and probabilistic depth refinement modules.

Interestingly, the threshold learning can also be beneficial to improve the performance of existing stereo confidence estimation approaches [37, 24]. The confidence map obtained from the existing approaches [37, 24] is refined through the soft-thresholding function controlled by the learned threshold. As shown in Fig. 2, the soft-thresholding function attenuates low confidence values that are less than the learned threshold τ to become as close as 0 while amplifying high confidence values to converge to 1. We validate through experiments that this process improves the prediction accuracy of the existing confidence estimation approaches. To sum up, our contributions are as follows.

- We propose a novel framework of monocular depth estimation using pseudo depth labels generated from self-supervised stereo matching methods.
- We introduce the threshold network that adaptively learns the threshold of the confidence map for better predicting the reliability of the inaccurate pseudo depth labels.
- The monocular depth map is further refined through the probabilistic refinement module based on the PAC layer.
- It is shown that the threshold network can also be used to enhance the prediction accuracy of existing confidence estimation approaches.

2. Related Work

Monocular depth estimation. Eigen *et al.* [7] initiated the monocular depth estimation through deep network that regresses a depth map with ground-truth depth information, inspiring numerous approaches based on multi-scale images [30], up-projection technique [28], motion parallax [49], ordinal regression [8], and semantic divide-and-conquer [50]. Despite remarkable performance over classical handcrafted approaches, they rely on abundant and high-quality ground-truth depth maps, which is costly to obtain.

To overcome this limitation, self-supervised learning has been introduced by leveraging other forms of supervision from stereo images and video sequences instead of ground

truth depth maps. Garg *et al.* [10] used the stereo photometric reprojection. Godard *et al.* [12] further used the left-right consistency between stereo images. Zhou *et al.* [55] proposed to leverage multi-view synthesis procedure, and this idea was extended using the feature-based warping loss in [54]. To take advantages of both supervised and self-supervised learning methods, semi-supervised learning methods have also been presented. Kuznietsov *et al.* [27] directly combined supervised and unsupervised loss terms. Ji *et al.* [21] utilizes an image-depth pair discriminator with a small amount of labeled dataset, alleviating the reliance on supervision. Recently, Gonzalebello *et al.* [14] proposed mirrored exponential disparity (MED) probability volumes to handle occluded areas.

The most related to our work is the methods of Guo *et al.* [17], Cho *et al.* [5], and Tonioni *et al.* [45] in which a stereo matching knowledge is distilled to train a monocular depth network. Since the disparity map estimated by stereo matching inherently contain unreliable ones, they used stereo confidence to build a pseudo-ground-truth disparity map by thresholding the confidence. Guo *et al.* [17] used a handcrafted occlusion map sensitive to outliers. Cho *et al.* [5] used a fixed threshold empirically, but it is ineffective to use the same threshold for all images. Unlike this, Tonioni *et al.* [45] tried to learn the threshold by using an additional regularization term that allows it to be between 0 and 1, but it is also difficult to learn the appropriate threshold with the implicit constraint by the regularization term. In our method, effective threshold learning is the main contribution.

Stereo confidence estimation. In parallel with the development of predicting depth from images, stereo confidence estimation has also been actively studied. Machine learning approaches [34, 43, 25] relying on shallow classifier, e.g., random tree [1], enable one to classify correct and incorrect pixels. Recently, deep convolutional neural network (CNN)-based approaches have become a mainstream. Various methods have been proposed that use the single- or bi-modal input, e.g., disparity [37], left and right disparities [40], 3D matching cost [41], 3D matching cost and disparity [26], and disparity and color image [48, 9]. Kim *et al.* [24] proposed to make full use of the tri-modal input in conjunction with locally adaptive attention and scale networks, achieving state-of-the-art prediction accuracy. All of these techniques require ground truth depth maps and have been used to refine a depth (or disparity) map with a fixed threshold which is set empirically. Poggi *et al.* [36] introduced a method for learning self-supervised confidence measure with various criterions.

3. Proposed Method

Unlike recent self-supervised monocular depth estimation approaches [10, 12, 31, 13, 35], we leverage the *pseudo*

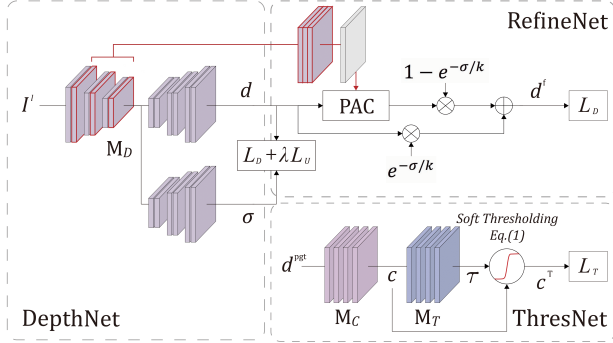


Figure 1. The proposed architecture consisting of ThresNet, DepthNet, and RefineNet. Given a pair of stereo images, the pseudo ground truth depth map d^{pgt} is precomputed using a self-supervised stereo matching network. The proposed model training begins with d^{pgt} by computing its confidence map c and the threshold τ through the ThresNet. The thresholded confidence map c^{T} is obtained using the soft-thresholding function. The DepthNet that infers the monocular depth map d and uncertainty map σ is trained by minimizing an objective defined using d^{pgt} filtered out by c^{T} . The monocular depth map d is finally refined through the probabilistic refinement module based on the pixel-adaptive convolution (PAC) layer in the RefineNet.

depth labels from a pair of stereo images as supervision for monocular depth estimation. Fig. 1 shows the overall procedure of the proposed method consisting of three networks, including DepthNet, RefineNet, and ThresNet.

The proposed model training begins with the pseudo depth labels d^{pgt} precomputed using the self-supervised stereo matching method [52]. Note that among various options provided in [52] for data synthesis, we adopted ‘Monodepth2’ [13] which is self-supervised monocular depth network. Its confidence map c is estimated by the confidence estimation module M_C , aiming at preventing the abuse of erroneous depth values in training the monocular depth network. To take into account the prediction errors of the confidence map itself, we further learn the threshold τ , truncating the confidence map, adaptively through the threshold module M_T . The thresholded confidence map c^{T} is obtained via the soft-thresholding by the learned threshold τ . This operation encourages to trust the pixel with a higher confidence value than a specific τ value. The DepthNet is trained by minimizing an objective defined using the pseudo depth labels d^{pgt} filtered out by the thresholded confidence map c^{T} . Finally, our method refines the monocular depth map d through the probabilistic refinement module based on the PAC layer [44] in the RefineNet.

3.1. Network Architecture

3.1.1 ThresNet

The ThresNet predicts the confidence map of the inaccurate pseudo depth label and its threshold in an adaptive man-

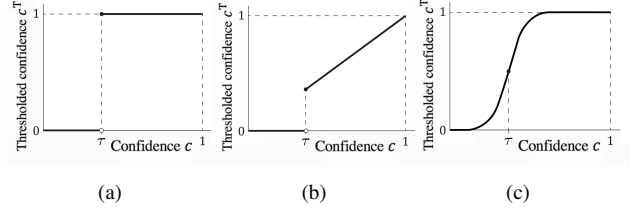


Figure 2. Comparison of confidence thresholding operator: (a) hard-thresholding used in [5], (b) hard-thresholding function used in [45], and (c) our soft-thresholding function in (1). The learned threshold is used in (b) and (c), while the threshold is fixed in (a) for all training images.

ner and then generates the thresholded confidence map via the soft-thresholding function. For the confidence estimation network M_C , we adopted the CCNN [37] thanks to its simplicity, but more sophisticated models [37, 24, 48] can also be utilized as a backbone. The threshold network M_T consists of four convolutional layers, followed by global average pooling and 1×1 convolution.

The estimated confidence map c is modulated by the threshold τ , such that a depth value with a higher confidence value than a specific τ value assumes to be trustworthy. A key issue is how to set accordingly τ which needs to vary depending on images. This threshold τ should be set low in the image where depth inference is easy while being set high in the opposite case (see Fig. 3). We approximate the thresholding operation with a smooth, differentiable function. The thresholded confidence map c^{T} is computed using the differentiable soft-thresholding function as follows:

$$c_p^{\text{T}}(\tau) = \frac{1}{1 + e^{-\varepsilon \cdot (c_p - \tau)}}, \quad (1)$$

where p represents a pixel. The slope of the thresholded confidence map c^{T} is adjusted by a hyperparameter ε , which is a positive constant. Too large ε changes the soft-thresholding function too rapidly (e.g. $\varepsilon = 90$), often making it non-differentiable. We set $\varepsilon = 10$ in experiments. The pixel-varying confidence map is transformed with the per-image threshold τ . We also investigated a pixel-varying threshold map τ_p , but its performance gain was negligible.

Fig. 2 compares the confidence thresholding functions. In Fig. 2 (a), the confidence threshold τ is fixed with a predefined value for all training images without considering image characteristics, often causing inaccurate pseudo depth values to be used during training. In Fig. 2 (b), it is learned using an additional regularization term [45], but its performance gain on the monocular depth estimation is rather limited, as reported in the original paper [45]. The proposed differential soft-thresholding function, controlled by the threshold τ dynamically conditioned on the pseudo depth map, leads to superior performance on the monocular depth estimation, when the threshold loss L_T is used

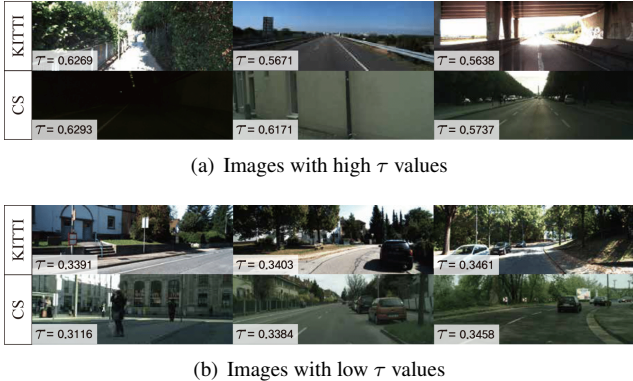


Figure 3. Examples of learned threshold τ by our threshold learning. CS indicates the Cityscapes dataset.

together. The ablation study of the confidence thresholding operators is provided in experiments.

Fig. 3 presents the estimation results of the ThresNet for the KITTI and Cityscapes datasets [6]. The threshold τ becomes higher in images where stereo matching do not work well, and vice versa. This indicates that the ThresNet is beneficial to improving the monocular depth network by excluding unreliable pseudo depth values effectively.

3.1.2 DepthNet and RefineNet

The DepthNet and RefineNet infer and refine the monocular depth map by leveraging the pseudo depth labels, masked out by the thresholded confidence map, as supervision. The DepthNet is based on the encoder-decoder architecture [38], in which an encoder takes an image and two decoders estimate the monocular depth map d and its uncertainty map σ . The uncertainty map, indicating the variance of the predicted monocular depth map, becomes higher when the prediction is unreliable, and vice versa. The encoder network consists of the first 13 convolution layers of the VGG network [42], and the decoder is symmetrical with the encoder. The uncertainty map σ is used to refine the monocular depth map in the subsequent RefineNet.

We first upsample L feature maps (here $L = 4$) from the encoder of the DepthNet to an original resolution and concatenate them. The concatenated features are then fused by passing through 1×1 convolution, generating a guidance feature g . The estimated monocular depth map d is finally fed into the PAC layer [44] with the guidance of the feature map g . Unlike the original PAC module that directly infers refined results, we leverage the residual connection that takes into account the uncertainty map σ for predicting the refined monocular depth map d^f such that

$$d^f = e^{-\sigma/k} \cdot d + (1 - e^{-\sigma/k})d' \quad (2)$$

where d' indicates the output of the PAC layer. k is a hyperparameter to control the refinement through the PAC layer,

and it was set to 1.

It should be noted that though some monocular depth estimation approaches [35, 2] have attempted to measure the uncertainty of the monocular depth estimation through deep network, our method proposes to infer the uncertainty map and use it for a subsequent refinement module. This framework can also be extended into various pixel-level labeling tasks based on the uncertainty prediction.

3.2. Loss Functions

3.2.1 Thresholding loss

The ThresNet with confidence and threshold networks can be trained in a supervised manner [37] or a self-supervised manner [36]. For the supervised training, we propose to use the sparse ground truth depth data provided by public benchmarks. For instance, we can leverage extremely sparse LiDAR depth maps of 3% density provided with a set of stereo image pairs in the KITTI dataset. The ground truth of the thresholded confidence map is generated using the sparse ground truth depth data like existing confidence estimation approaches [24] and this is used to train the ThresNet using a cross-entropy loss L_T . More details on the ground truth confidence map are provided in the supplementary material. Alternatively, the ThresNet can be trained in the self-supervised manner without using the LiDAR depth maps. Following [36], we generate the pseudo ground truth of the thresholded confidence map according to various criteria (e.g., reprojection error, disparity agreement). The loss L_T for the self-supervised training is defined as a multi-modal binary cross entropy loss of [36]. In Table 1, we compare the monocular depth accuracy when using the supervised and self-supervised ThresNets, and found the accuracy is almost similar.

In [45], the threshold is also learned to exclude depth values with low confidences when training their network. It was reported that when using the depth regression loss only, the threshold τ would converge to 1 for masking out all pixels [45]. Thus, they propose to include an additional regularization loss, $-\log(1 - \tau)$, that prevents the threshold τ from approaching 1. Though this term allows τ to be between 0 and 1, it does not guarantee to yield accurate prediction results of the threshold τ . Contrastingly, our method attempts to learn the threshold τ with the soft-thresholding function and the explicit supervision. We will verify the effectiveness of our threshold learning approach in the ablation study of Table 4.

3.2.2 Depth regression loss

A monocular depth map from the DepthNet is leveraged to compute a confidence-guided depth regression loss L_D

assisted by the thresholded confidence map c^T as follows:

$$L_D = \frac{1}{Z} \sum_{p \in \Omega} c_p^T(\tau) \cdot |d_p - d_p^{\text{pgt}}|, \quad (3)$$

where d and d^{pgt} indicate the predicted depth map and pseudo ground truth depth map, respectively. Ω represents a set of all pixels. The loss L_D is normalized with $Z = \sum_{p \in \Omega} c_p^T(\tau)$.

Additionally, we leverage the negative log-likelihood minimization to infer the uncertainty of the network output. The predictive distribution of the network output d can be modelled as the Laplacian likelihood [23, 20, 22] as follows:

$$L_U = \frac{1}{|\Omega|} \sum_{p \in \Omega} \left(\frac{|d_p - d_p^{\text{pgt}}|}{\sigma_p} + \log \sigma_p \right), \quad (4)$$

where the variance σ represents the uncertainty map of the predicted depth map. The logarithmic term $\log \sigma$ prevents σ from approaching to infinity [23]. We combine two losses L_D , taking into account the reliability of the pseudo ground truth depth map d^{pgt} , and L_U predicting the uncertainty of the predicted depth map d , such that

$$L = L_D + \lambda L_U, \quad (5)$$

where λ represents hyperparameter that balances two losses which is experimentally determined to 10^{-3} . This enables for modeling the uncertainty of the monocular depth estimation network while considering the confidence of the pseudo depth label. As shown in Fig. 1, the DepthNet that infers both the monocular depth map and uncertainty map is trained with L in (5), while the RefineNet leverages L_D in (3) as it predicts the final monocular depth map only.

3.3. Training Details

In our work, the DepthNet and RefineNet are trained simultaneously by minimizing L and L_D , while the ThresNet consisting of confidence and threshold networks is trained solely by minimizing L_T , similar to existing confidence estimation approaches [37, 34, 43, 24]. Though the whole networks can be trained end-to-end, we found through experiments that the performance gain over the separate training is relatively marginal.

It has been reported in literature [37, 48] that the confidence network trained with one dataset exhibits a good generalization capability for another dataset. In a similar context, our confidence and threshold networks trained with the KITTI dataset show satisfactory generalization capability for different datasets. Taking these into account, we transfer the knowledge learned from one dataset to another. To be specific, when only stereo image pairs are available for training (e.g. Cityscape dataset), the DepthNet and RefineNet are trained via the minimization of L and L_D , with

the ThresNet being frozen with the parameters trained with the KITTI dataset. As shown in Fig. 3, the ThresNet trained with the KITTI dataset produces appropriate thresholds for both the KITTI and Cityscape datasets.

4. Extension to Confidence Estimation

The soft-thresholding attenuates low confidence values that are less than τ to become as close as 0 while amplifying high confidence values to converge to 1. It reduces the number of ambiguous pixels to determine the reliability, for which a confidence value is far from 0 or 1. We discuss how the soft-thresholding based on the threshold network can improve the prediction accuracy of existing confidence estimation approaches [37, 24]. In the ThresNet of Fig. 1, the confidence network can be replaced with the existing confidence estimation approaches. One difference is that the loss L_T (cross-entropy loss) is measured on the disparity domain, considering that the existing confidence estimation approaches are trained on the disparity domain. This formulation is model-agnostic, and any kind of existing confidence estimation approaches can be used in a plug-and-play fashion.

5. Experimental results

5.1. Implementation details

The proposed method was implemented in PyTorch framework and run Titan RTX GPU. We trained the whole networks on the learning rate of 10^{-4} and batches of 32 images resized to 192×480 for 30 epochs. We trained the proposed monocular depth estimation network consisting of DepthNet and RefineNet on the standard 20k stereo images provided in the KITTI dataset. We evaluate our methods on following five metrics ‘RMSE’, ‘RMSE log’, ‘Abs Rel’, ‘Sq. Rel’, and ‘Accuracy’, proposed in Eigen *et al.* [7].

5.2. Evaluation on monocular depth estimation

5.2.1 KITTI

In Table 1, we evaluated the monocular depth estimation performance quantitatively on the KITTI Eigen Split [7] dataset with setting maximum depth to 80 meters with Gargs crop [10]. A comprehensive evaluation was conducted with Monodepth [12], Uncertainty [35], MonoResMatch [47], Monodepth2 [13], DepthHint [51], PackNet-SfM [16], and Insta-DM [29]. For the training data, ‘S’ indicates using stereo images for self-supervised monocular depth estimation. ‘M’ represents a monocular video sequence. The evaluation of the proposed method is twofold; ‘Ours (D)’ trained with only the DepthNet using L_D in (3) without refining the depth map, and ‘Ours (D+R)’ trained with the DepthNet and RefineNet.

Table 1. Quantitative evaluation for depth estimation with existing methods on KITTI Eigen Split [7] dataset. Numbers in bold and underlined represent 1st and 2nd ranking, respectively. ‘Ours[†]’ is obtained using the self-supervised ThresNet [36], while ‘Ours’ indicates the results obtained using the supervised ThresNet.

Method	Data	#p	time	Lower is better				Accuracy: higher is better		
				Abs Rel	Sqr Rel	RMSE	RMSE log	$\delta < 1.25$	$\delta < 1.25^2$	$\delta < 1.25^3$
Monodepth [12]	S	56M	9.4ms	0.138	1.186	5.650	0.234	0.813	0.930	0.969
Monodepth2 [13]	S	14M	2.9ms	0.108	0.842	4.891	0.207	0.866	0.949	0.976
Uncertainty [35]	S	14M	3.6ms	0.107	0.811	4.796	0.200	0.866	0.952	0.978
MonoResMatch [47]	S	41M	8.3ms	0.111	0.867	4.714	0.199	0.864	0.954	0.979
DepthHint [51]	S	33M	6.6ms	0.102	0.762	4.602	0.189	0.880	<u>0.960</u>	<u>0.981</u>
PackNet-SfM [16]	M	122M	9.5ms	0.111	0.785	4.601	0.189	0.878	<u>0.960</u>	0.982
Insta-DM [29]	M	14M	3.0ms	0.112	0.777	4.772	0.191	0.872	0.959	0.982
Ours (D)	S	28M	6.8ms	<u>0.099</u>	0.652	4.266	0.187	<u>0.883</u>	<u>0.960</u>	<u>0.981</u>
Ours (D+R)	S	42M	8.2ms	0.096	<u>0.627</u>	4.201	<u>0.186</u>	0.885	0.961	0.982
Ours [†] (D)	S	28M	6.8ms	0.100	<u>0.644</u>	4.251	0.187	0.882	<u>0.960</u>	<u>0.981</u>
Ours [†] (D+R)	S	42M	8.2ms	0.098	0.621	<u>4.215</u>	0.185	0.885	0.961	0.982

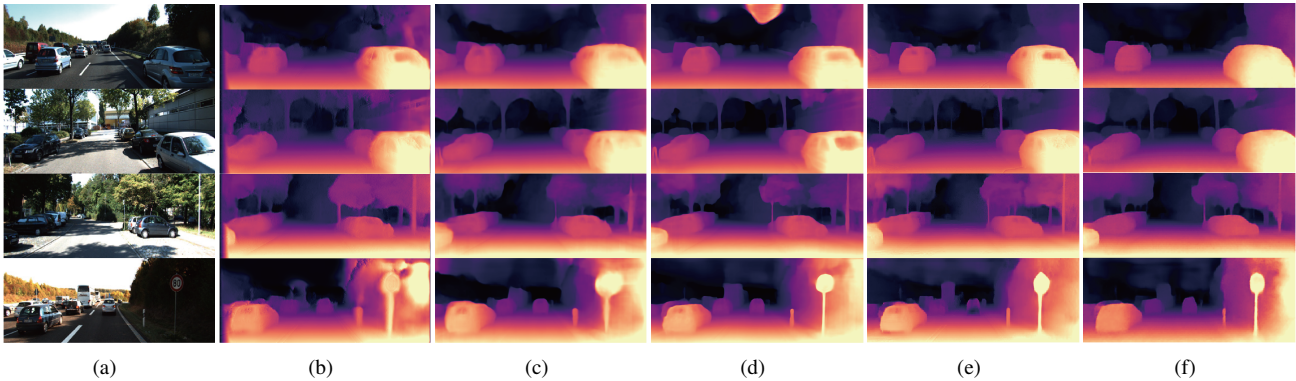


Figure 4. Qualitative evaluation with existing monocular depth estimation methods on the Eigen Split [7] of KITTI dataset: (a) input image, (b) Monodepth [12], (c) Monodepth2 [13], (d) DepthHint [51], (e) PackNet-SfM [16] and (f) Ours (D+R).

As reported in Table 1, although ‘Ours (D)’ leverages a rather simple encoder-decoder architecture, it achieves the superior performance over existing methods, demonstrating the effectiveness of the proposed threshold learning approach. In ‘Ours (D+R)’, the monocular depth accuracy was further improved by making use of the probabilistic refinement module based on the uncertainty map and the PAC layer in the RefineNet. We also evaluated the number of parameters used and an inference time, noted as ‘#p’ and ‘time’, respectively. Our method uses relatively smaller or similar number of parameters compared to other methods. ‘Ours[†]’ is obtained using the self-supervised ThresNet [36], while ‘Ours’ indicates the results obtained using the supervised ThresNet. We found that their monocular depth accuracy is almost similar. The following results including ablation study were conducted with the supervised ThresNet. Fig. 4 shows the qualitative comparison with existing methods on the KITTI Eigen Split [7] dataset. It was shown that the proposed method recovers complete instances better while preserving fine object boundaries.

5.3. Cityscapes

We also evaluated the performance of the proposed method on the Cityscapes dataset. The Cityscapes dataset provides only stereo images without the ground truth, and thus the ThresNet trained with the KITTI dataset was used to infer the threshold. Table 2 shows the quantitative evaluation on Cityscapes dataset [6] with the DepthNet and RefineNet fine-tuned on the Cityscapes dataset, while the ThresNet is frozen. We compared our results with Monodepth2 [13], DepthHint [51] and PackNet-SfM [16]. We set maximum depth to 80 meters with the per-image median scaling approach [55]. We used the SGM depth [18] as ground truth for the evaluation. The outstanding performance of our method supports the claim that the ThresNet trained with the KITTI dataset shows a satisfactory generalization capability for different datasets.

5.4. Evaluation on uncertainty estimation

To evaluate the performance of the uncertainty measure, we use sparsification plots used in [20]. ‘AUSE’ denotes the Area Under the Sparsification Error which quantifies how

Table 2. Quantitative evaluation for monocular depth estimation results on Cityscapes validation dataset with fine-tuning on Cityscapes training dataset. Numbers in bold and underlined represent 1st and 2nd ranking, respectively.

Method	Data	Lower is better				Accuracy: higher is better		
		Abs Rel	Sqr Rel	RMSE	RMSE log	$\delta < 1.25$	$\delta < 1.25^2$	$\delta < 1.25^3$
Monodepth2 [13]	S	0.124	1.287	7.293	0.223	0.785	0.947	0.981
Struct2Depth [4]	M	0.145	1.737	7.280	0.205	0.813	0.942	0.978
DepthHint [51]	S	0.128	1.268	7.156	0.218	0.812	0.949	0.982
Gordon [15]	M	0.127	1.330	6.960	0.195	0.830	0.947	0.981
Ours (D)	S	<u>0.123</u>	<u>1.141</u>	<u>6.735</u>	0.204	0.844	<u>0.962</u>	<u>0.985</u>
Ours (D+R)	S	0.115	1.125	6.584	0.195	0.857	0.963	0.986

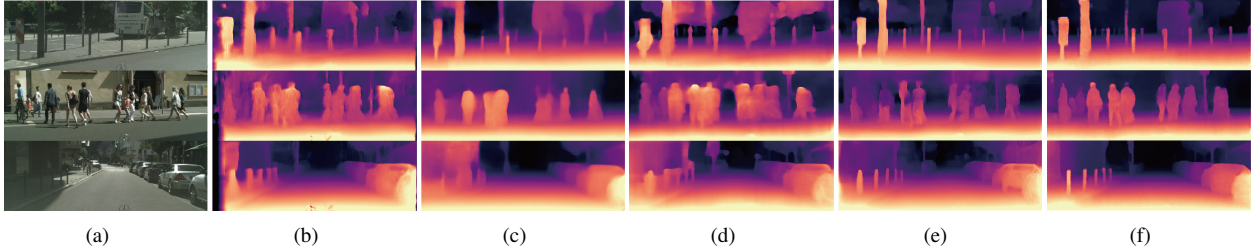


Figure 5. Qualitative evaluation for depth estimation with existing methods on Cityscapes validation dataset: (a) Input image, (b) Monodepth [12], (c) MonoResMatch [47], (d) DepthHint [51], (e) PackNet-SfM [16] (f) Ours (D+R).

close the estimate is to the oracle uncertainty, which is **lower** the better. ‘AURG’ denotes the Area Under the Random Gain, which indicates how better it is compared to the case without modelling, which is **higher** the better. In Table 3, the uncertainty measure estimated by the proposed method was compared with ‘Monodepth2-Log’ of Poggi *et al.* [35], trained under the same setup as our experiments.

5.5. Ablation study

Threshold learning In Table 4, we conducted the ablation study to validate the performance improvement by the proposed threshold learning over existing thresholding approaches [5, 45]. For a fair comparison, we obtained the results using the monocular depth network trained with only the DepthNet (without the uncertainty decoder), when varying thresholding functions. ‘Baseline’ represents the results obtained using the confidence map without thresholding. The results of [5] were obtained using the hard thresholding of Fig. 2 (a) with $\tau = 0.3$, following the setup of [5]. The performance of [5, 45] was almost similar, though the method in [45] learned the threshold τ with the thresholding function of Fig. 2 (b). We found that the regularization loss $-\log(1 - \tau)$ [45], used to prevent the threshold τ from approaching 1, does not generate a meaningful variant for the learned threshold due to the lack of explicit supervision for the threshold learning. ‘Tonioni *et al.* [45] + L_T ’ were obtained using the thresholding function of Fig. 2 (b) and our loss L_T . The performance gain over ‘Tonioni *et al.* [45]’ demonstrates the effectiveness of L_T . ‘Ours (D)’ achieves a substantial performance gain, demonstrating the effectiveness of the proposed threshold learning with L_T .

Table 3. Quantitative evaluation for uncertainty estimation with the state-of-the-art method on KITTI Eigen Split [7] dataset. Numbers in bold indicate the better performance.

Method	Abs Rel		RMSE		$\delta \geq 1.25$	
	AUSE	AURG	AUSE	AURG	AUSE	AURG
Uncertainty [35]	0.022	0.036	0.938	2.402	0.018	0.061
Ours	0.021	0.048	0.765	2.881	0.025	0.080

Adaptability We also validated the effectiveness of our method when applied to different network architectures, e.g., PackNet [16]. Table 5 shows quantitative evaluation results when using our confidence threshold learning and probabilistic refinement on the PackNet architecture. ‘PackNet (D)’ represents the results obtained using the DepthNet only, whereas ‘PackNet (D+R)’ is the results using both DepthNet and RefineNet. We observed that our framework also improves the monocular depth accuracy for the PackNet architecture.

Uncertainty To evaluate the importance of using the estimated uncertainty in the RefineNet, we compared the results obtained using the proposed depth refinement of (2) and the simple depth refinement ($d^f = d + d'$) without σ in Table 6, demonstrating the effectiveness of the depth refinement based on the uncertainty map.

Pseudo ground truth depth labels So far, all experiments were conducted with the self-supervised pseudo depth maps obtained using [52]. To validate the adaptability of our framework with respect to the pseudo depth labels, we performed additional experiments with the pseudo ground truth depth maps generated by [46], which are trained with synthetic data and fine-tuned with an self-supervised recon-

Table 4. Comparison with other thresholding methods on the KITTI Eigen Split [7] dataset. We evaluated the performance with the supervised ThresNet, and L_T is a cross-entropy loss.

	τ	Abs	RMSE	$\delta < 1.25$
Baseline	\times	0.108	4.552	0.869
Cho et al. [5]	fixed	0.102	4.441	0.874
Tonioni et al. [45]	learned	0.101	4.453	0.878
Tonioni et al. [45] + L_T	learned	0.100	4.390	0.879
Ours (D)	learned	0.099	4.266	0.883

Table 5. Quantitative evaluation of the results obtained by applying our threshold learning and probabilistic refinement to the PackNet-SfM architecture [16] on the KITTI Eigen Split [7] dataset.

	Abs	RMSE	$\delta < 1.25$
PackNet-SfM [16]	0.111	4.601	0.878
PackNet-SfM (D)	0.105	4.258	0.880
PackNet-SfM (D+R)	0.100	4.225	0.883

Table 6. Ablation study of the uncertainty map.

	Abs	Sqr	RMSE	RMSE log	$\delta < 1.25$
(2) w/o σ	0.099	0.661	4.298	0.188	0.881
(2)	0.096	0.627	4.201	0.186	0.885

Table 7. Quantitative evaluation when using pseudo depth labels generated by [46] on the KITTI Eigen Split [7] dataset.

	Abs	Sqr	RMSE	RMSE log	$\delta < 1.25$
Ours (D)	0.102	0.728	4.281	0.189	0.880
Ours (D+R)	0.100	0.711	4.230	0.187	0.883

struction loss with meta-learning framework. Table 7 shows that the monocular depth accuracy is still superior to state-of-the-arts monocular depth estimation approaches.

5.6. Confidence evaluation

We validated the effectiveness of the proposed threshold learning in terms of confidence prediction accuracy by applying it to two confidence estimation approaches, CCNN [37] and LAFNet [24]. We trained the two confidence estimation methods with 20 out of 194 images provided in the KITTI 2012 training dataset [11]. Note that the confidence estimation approaches [37, 24] are evaluated by training them in a supervised manner. The area under the curve (AUC) [19], which is a common metric for confidence estimation approaches, was used for an objective evaluation. Refer to the supplementary material for details on measuring AUC and optimal AUC and more results. Following confidence estimation literatures, input disparity maps used for predicting the confidence maps were obtained using two popular stereo algorithms, ‘Census-SGM’ [18] and ‘MC-CNN’ [53].

Table 8 shows objective evaluation results for 200 images of KITTI 2015 dataset [32] and 15 images of Middlebury v3 dataset [39]. ‘w/ τ ’ denotes our results using the

Table 8. Performance evaluation of confidence estimation for KITTI 2015 and Middlebury v3 datasets with two popular stereo matching methods C-SGM (Census-SGM) [18] and MC-CNN [53]. AUC values are reported and the lower is the better.

	KITTI 2015		MID 2014	
	C-SGM / MC-CNN		C-SGM / MC-CNN	
	C-SGM	MC-CNN	C-SGM	MC-CNN
CCNN	1.868 / 3.190	9.486 / 9.787		
CCNN w/ τ	1.720 / 3.525	8.314 / 9.497		
LAFNet*	1.797 / 3.051	8.895 / 9.660		
LAFNet* w/ τ	1.687 / 3.037	8.988 / 9.456		
LAFNet	1.680 / 2.903	8.884 / 9.305		
LAFNet w/ τ	1.587 / 2.885	8.680 / 8.622		
optimal	0.737 / 2.761	3.887 / 4.985		

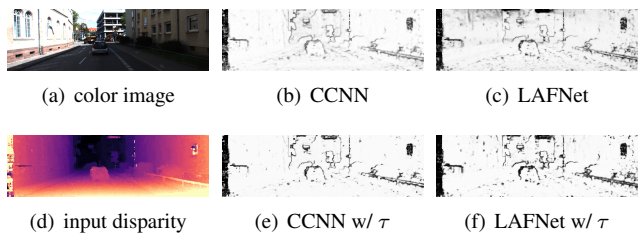


Figure 6. Qualitative results of confidence map on KITTI 2015 dataset using census-SGM.

soft-thresholding technique. LAFNet* denotes the LAFNet [24] in which 3D cost volume is not used as an input. Our approach consistently outperforms the original confidence estimation methods, demonstrating the effectiveness of the proposed threshold learning. Fig. 6 compares the confidence maps visually. While the original confidence maps contain ambiguous values for which it is difficult to determine whether the depth label is correct, our thresholded confidence map yields more distinct values that are close to 0 or 1. Such a binarization enables the estimated confidence to have similar distribution to ground truth confidence, thus improving a discriminative power.

6. Conclusion

In this work, we have proposed a novel framework for monocular depth estimation based on pseudo depth labels generated by self-supervised stereo matching methods. The confidence map is used to exclude erroneous depth values within the pseudo depth labels. The prediction errors in the confidence map are further suppressed by making use of the soft-thresholding based on threshold learning. Furthermore, the probabilistic refinement module enables improving the monocular depth accuracy with the help of the uncertainty map. The proposed framework has shown impressive performances over state-of-the-arts on several popular datasets. It was also shown that threshold learning can also boost the prediction accuracy of existing confidence approaches.

References

- [1] Leo Breiman. Random forests. *Machine learning*, 45(1):5–32, 2001. 2
- [2] Fabian Brickwedde, Steffen Abraham, and Rudolf Mester. Mono-sf: Multi-view geometry meets single-view depth for monocular scene flow estimation of dynamic traffic scenes. In *Proceedings of the IEEE International Conference on Computer Vision*, pages 2780–2790, 2019. 4
- [3] Yuanzhouhan Cao, Zifeng Wu, and Chunhua Shen. Estimating depth from monocular images as classification using deep fully convolutional residual networks. *IEEE Transactions on Circuits and Systems for Video Technology*, 28(11):3174–3182, 2017. 1
- [4] Vincent Casser, Soeren Pirk, Reza Mahjourian, and Anelia Angelova. Unsupervised monocular depth and ego-motion learning with structure and semantics. In *CVPR Workshop on Visual Odometry and Computer Vision Applications Based on Location Cues (VOCVALC)*, 2019. 7
- [5] Jaehoon Cho, Dongbo Min, Youngjung Kim, and Kwanghoon Sohn. A large rgb-d dataset for semi-supervised monocular depth estimation. *arXiv preprint arXiv:1904.10230*, 2019. 1, 2, 3, 7, 8
- [6] Marius Cordts, Mohamed Omran, Sebastian Ramos, Timo Rehfeld, Markus Enzweiler, Rodrigo Benenson, Uwe Franke, Stefan Roth, and Bernt Schiele. The cityscapes dataset for semantic urban scene understanding. In *Proceedings of the IEEE conference on computer vision and pattern recognition*, pages 3213–3223, 2016. 4, 6
- [7] David Eigen, Christian Puhrsch, and Rob Fergus. Depth map prediction from a single image using a multi-scale deep network. In *Advances in neural information processing systems*, pages 2366–2374, 2014. 1, 2, 5, 6, 7, 8
- [8] Huan Fu, Mingming Gong, Chaohui Wang, Kayhan Batmanghelich, and Dacheng Tao. Deep ordinal regression network for monocular depth estimation. In *Proceedings of the IEEE Conference on Computer Vision and Pattern Recognition*, pages 2002–2011, 2018. 2
- [9] Zehua Fu and Mohsen Ardabilian Fard. Learning confidence measures by multi-modal convolutional neural networks. In *2018 IEEE Winter Conference on Applications of Computer Vision (WACV)*, pages 1321–1330. IEEE, 2018. 2
- [10] Ravi Garg, Vijay Kumar Bg, Gustavo Carneiro, and Ian Reid. Unsupervised cnn for single view depth estimation: Geometry to the rescue. In *European conference on computer vision*, pages 740–756. Springer, 2016. 1, 2, 5
- [11] Andreas Geiger, Philip Lenz, Christoph Stiller, and Raquel Urtasun. Vision meets robotics: The kitti dataset. *The International Journal of Robotics Research*, 32(11):1231–1237, 2013. 8
- [12] Clément Godard, Oisín Mac Aodha, and Gabriel J Brostow. Unsupervised monocular depth estimation with left-right consistency. In *Proceedings of the IEEE Conference on Computer Vision and Pattern Recognition*, pages 270–279, 2017. 1, 2, 5, 6, 7
- [13] Clément Godard, Oisín Mac Aodha, Michael Firman, and Gabriel J Brostow. Digging into self-supervised monocular depth estimation. In *Proceedings of the IEEE international conference on computer vision*, pages 3828–3838, 2019. 1, 2, 3, 5, 6, 7
- [14] Juan Luis GonzalezBello and Munchurl Kim. Forget about the lidar: Self-supervised depth estimators with med probability volumes. *Advances in Neural Information Processing Systems*, 33:12626–12637, 2020. 2
- [15] Ariel Gordon, Hanhan Li, Rico Jonschkowski, and Anelia Angelova. Depth from videos in the wild: Unsupervised monocular depth learning from unknown cameras. In *Proceedings of the IEEE International Conference on Computer Vision*, pages 8977–8986, 2019. 7
- [16] Vitor Guizilini, Rares Ambrus, Sudeep Pillai, Allan Raveentos, and Adrien Gaidon. 3d packing for self-supervised monocular depth estimation. In *Proceedings of the IEEE/CVF Conference on Computer Vision and Pattern Recognition*, pages 2485–2494, 2020. 5, 6, 7, 8
- [17] Xiaoyang Guo, Hongsheng Li, Shuai Yi, Jimmy Ren, and Xiaogang Wang. Learning monocular depth by distilling cross-domain stereo networks. In *Proceedings of the European Conference on Computer Vision (ECCV)*, pages 484–500, 2018. 2
- [18] Heiko Hirschmüller. Accurate and efficient stereo processing by semi-global matching and mutual information. In *2005 IEEE Computer Society Conference on Computer Vision and Pattern Recognition (CVPR'05)*, volume 2, pages 807–814. IEEE, 2005. 6, 8
- [19] Xiaoyan Hu and Philippos Mordohai. A quantitative evaluation of confidence measures for stereo vision. *IEEE transactions on pattern analysis and machine intelligence*, 34(11):2121–2133, 2012. 8
- [20] Eddy Ilg, Ozgun Cicek, Silvio Galesso, Aaron Klein, Osama Makansi, Frank Hutter, and Thomas Brox. Uncertainty estimates and multi-hypotheses networks for optical flow. In *Proceedings of the European Conference on Computer Vision (ECCV)*, pages 652–667, 2018. 5, 6
- [21] Rongrong Ji, Ke Li, Yan Wang, Xiaoshuai Sun, Feng Guo, Xiaowei Guo, Yongjian Wu, Feiyue Huang, and Jiebo Luo. Semi-supervised adversarial monocular depth estimation. *IEEE transactions on pattern analysis and machine intelligence*, 2019. 2
- [22] Alex Kendall and Yarin Gal. What uncertainties do we need in bayesian deep learning for computer vision? *arXiv preprint arXiv:1703.04977*, 2017. 5
- [23] Alex Kendall, Yarin Gal, and Roberto Cipolla. Multi-task learning using uncertainty to weigh losses for scene geometry and semantics. In *Proceedings of the IEEE conference on computer vision and pattern recognition*, pages 7482–7491, 2018. 5
- [24] Sunok Kim, Seungryong Kim, Dongbo Min, and Kwanghoon Sohn. Laf-net: Locally adaptive fusion networks for stereo confidence estimation. In *Proceedings of the IEEE Conference on Computer Vision and Pattern Recognition*, pages 205–214, 2019. 2, 3, 4, 5, 8
- [25] Sunok Kim, Dongbo Min, Seungryong Kim, and Kwanghoon Sohn. Feature augmentation for learning confidence measure in stereo matching. *IEEE Transactions on Image Processing*, 26(12):6019–6033, 2017. 2

- [26] Sunok Kim, Dongbo Min, Seungryong Kim, and Kwanghoon Sohn. Unified confidence estimation networks for robust stereo matching. *IEEE Transactions on Image Processing*, 28(3):1299–1313, 2018. 2
- [27] Yevhen Kuznietsov, Jorg Stuckler, and Bastian Leibe. Semi-supervised deep learning for monocular depth map prediction. In *Proceedings of the IEEE conference on computer vision and pattern recognition*, pages 6647–6655, 2017. 2
- [28] Iro Laina, Christian Rupprecht, Vasileios Belagiannis, Federico Tombari, and Nassir Navab. Deeper depth prediction with fully convolutional residual networks. In *2016 Fourth international conference on 3D vision (3DV)*, pages 239–248. IEEE, 2016. 2
- [29] Seokju Lee, Sunghoon Im, Stephen Lin, and In So Kweon. Learning monocular depth in dynamic scenes via instance-aware projection consistency. In *Proceedings of the AAAI Conference on Artificial Intelligence (AAAI)*, 2021. 5, 6
- [30] Bo Li, Chunhua Shen, Yuchao Dai, Anton Van Den Hengel, and Mingyi He. Depth and surface normal estimation from monocular images using regression on deep features and hierarchical crfs. In *Proceedings of the IEEE conference on computer vision and pattern recognition*, pages 1119–1127, 2015. 1, 2
- [31] Yue Luo, Jimmy Ren, Mude Lin, Jiahao Pang, Wenxiu Sun, Hongsheng Li, and Liang Lin. Single view stereo matching. In *Proceedings of the IEEE Conference on Computer Vision and Pattern Recognition*, pages 155–163, 2018. 1, 2
- [32] Moritz Menze and Andreas Geiger. Object scene flow for autonomous vehicles. In *Proceedings of the IEEE conference on computer vision and pattern recognition*, pages 3061–3070, 2015. 8
- [33] Jiahao Pang, Wenxiu Sun, Jimmy SJ Ren, Chengxi Yang, and Qiong Yan. Cascade residual learning: A two-stage convolutional neural network for stereo matching. In *Proceedings of the IEEE International Conference on Computer Vision Workshops*, pages 887–895, 2017. 1
- [34] Min-Gyu Park and Kuk-Jin Yoon. Leveraging stereo matching with learning-based confidence measures. In *Proceedings of the IEEE Conference on Computer Vision and Pattern Recognition*, pages 101–109, 2015. 2, 5
- [35] Matteo Poggi, Filippo Aleotti, Fabio Tosi, and Stefano Mattoccia. On the uncertainty of self-supervised monocular depth estimation. In *Proceedings of the IEEE/CVF Conference on Computer Vision and Pattern Recognition*, pages 3227–3237, 2020. 1, 2, 4, 5, 6, 7
- [36] Matteo Poggi, Filippo Aleotti, Fabio Tosi, Giulio Zaccaroni, and Stefano Mattoccia. Self-adapting confidence estimation for stereo. In *Computer Vision–ECCV 2020: 16th European Conference, Glasgow, UK, August 23–28, 2020, Proceedings, Part XXIV 16*, pages 715–733. Springer, 2020. 2, 4, 6
- [37] Matteo Poggi and Stefano Mattoccia. Learning from scratch a confidence measure. In *BMVC*, 2016. 2, 3, 4, 5, 8
- [38] Olaf Ronneberger, Philipp Fischer, and Thomas Brox. U-net: Convolutional networks for biomedical image segmentation. In *International Conference on Medical image computing and computer-assisted intervention*, pages 234–241. Springer, 2015. 4
- [39] Daniel Scharstein, Heiko Hirschmüller, York Kitajima, Greg Krathwohl, Nera Nešić, Xi Wang, and Porter Westling. High-resolution stereo datasets with subpixel-accurate ground truth. In *German conference on pattern recognition*, pages 31–42. Springer, 2014. 8
- [40] Akihito Seki and Marc Pollefeys. Patch based confidence prediction for dense disparity map. In *BMVC*, volume 2, page 4, 2016. 2
- [41] Amit Shaked and Lior Wolf. Improved stereo matching with constant highway networks and reflective confidence learning. In *Proceedings of the IEEE Conference on Computer Vision and Pattern Recognition*, pages 4641–4650, 2017. 2
- [42] Karen Simonyan and Andrew Zisserman. Very deep convolutional networks for large-scale image recognition. *arXiv preprint arXiv:1409.1556*, 2014. 4
- [43] Aristotle Spyropoulos and Philippos Mordohai. Correctness prediction, accuracy improvement and generalization of stereo matching using supervised learning. *International Journal of Computer Vision*, 118(3):300–318, 2016. 2, 5
- [44] Hang Su, Varun Jampani, Deqing Sun, Orazio Gallo, Erik Learned-Miller, and Jan Kautz. Pixel-adaptive convolutional neural networks. In *Proceedings of the IEEE Conference on Computer Vision and Pattern Recognition*, pages 11166–11175, 2019. 2, 3, 4
- [45] Alessio Tonioni, Matteo Poggi, Stefano Mattoccia, and Luigi Di Stefano. Unsupervised domain adaptation for depth prediction from images. *IEEE transactions on pattern analysis and machine intelligence*, 2019. 1, 2, 3, 4, 7, 8
- [46] Alessio Tonioni, Oscar Rahnama, Thomas Joy, Luigi Di Stefano, Thalaiyasingam Ajanthan, and Philip HS Torr. Learning to adapt for stereo. In *Proceedings of the IEEE/CVF Conference on Computer Vision and Pattern Recognition*, pages 9661–9670, 2019. 7, 8
- [47] Fabio Tosi, Filippo Aleotti, Matteo Poggi, and Stefano Mattoccia. Learning monocular depth estimation infusing traditional stereo knowledge. In *Proceedings of the IEEE Conference on Computer Vision and Pattern Recognition*, pages 9799–9809, 2019. 5, 6, 7
- [48] Fabio Tosi, Matteo Poggi, Antonio Benincasa, and Stefano Mattoccia. Beyond local reasoning for stereo confidence estimation with deep learning. In *Proceedings of the European Conference on Computer Vision (ECCV)*, pages 319–334, 2018. 2, 3, 5
- [49] Benjamin Ummenhofer, Huizhong Zhou, Jonas Uhrig, Nikolaus Mayer, Eddy Ilg, Alexey Dosovitskiy, and Thomas Brox. Demon: Depth and motion network for learning monocular stereo. In *Proceedings of the IEEE Conference on Computer Vision and Pattern Recognition*, pages 5038–5047, 2017. 2
- [50] Lijun Wang, Jianming Zhang, Oliver Wang, Zhe Lin, and Huchuan Lu. Sdc-depth: Semantic divide-and-conquer network for monocular depth estimation. In *Proceedings of the IEEE/CVF Conference on Computer Vision and Pattern Recognition*, pages 541–550, 2020. 2
- [51] Jamie Watson, Michael Firman, Gabriel J Brostow, and Daniyar Turmukhambetov. Self-supervised monocular depth hints. In *Proceedings of the IEEE International Conference on Computer Vision*, pages 2162–2171, 2019. 5, 6, 7

- [52] Jamie Watson, Oisín Mac Aodha, Daniyar Turmukhambetov, Gabriel J Brostow, and Michael Firman. Learning stereo from single images. In *European Conference on Computer Vision*, pages 722–740. Springer, 2020. [3](#), [7](#)
- [53] Jure Žbontar and Yann LeCun. Stereo matching by training a convolutional neural network to compare image patches. *The journal of machine learning research*, 17(1):2287–2318, 2016. [8](#)
- [54] Huangying Zhan, Ravi Garg, Chamara Saroj Weerasekera, Kejie Li, Harsh Agarwal, and Ian Reid. Unsupervised learning of monocular depth estimation and visual odometry with deep feature reconstruction. In *Proceedings of the IEEE Conference on Computer Vision and Pattern Recognition*, pages 340–349, 2018. [2](#)
- [55] Tinghui Zhou, Matthew Brown, Noah Snavely, and David G Lowe. Unsupervised learning of depth and ego-motion from video. In *Proceedings of the IEEE Conference on Computer Vision and Pattern Recognition*, pages 1851–1858, 2017. [2](#), [6](#)

Adaptive confidence thresholding for monocular depth estimation - Supplementary material

Hyesong Choi^{1*}, Hunsang Lee^{2*}, Sunkyung Kim¹, Sunok Kim³,
Seungryong Kim⁴, Kwanghoon Sohn², Dongbo Min^{1†}

¹Ewha W. University, ²Yonsei University, ³Korea Aerospace University, ⁴Korea University

In this document, we provide more comprehensive results not provided in the original manuscript due to the page limit as below. The code to reproduce our results will be publicly available soon. Note that all experiments were conducted with the supervised ThresNet.

- Histogram of the learned threshold τ and qualitative evaluation of depth results computed using different thresholding methods (Section 1)
- Qualitative evaluation for monocular depth estimation with state-of-the-arts on KITTI and Cityscapes datasets (Section 2.2 and 2.3)
- Quantitative evaluation for monocular depth estimation on Cityscape dataset without fine-tuning (Section 2.4)
- Quantitative evaluation for monocular depth estimation using improved ground truth depth maps [22] on KITTI dataset (Section 2.5)
- Performance analysis according to a hyperparameter ϵ used in the soft-thresholding function (Section 2.6)
- Quantitative evaluation of the proposed method according to the use of DepthNet and RefineNet (Section 2.7)
- Ground truth confidence map and evaluation metric used in the confidence estimation (Section 3.1 and 3.2)
- Qualitative result for confidence estimation with state-of-the-arts on KITTI dataset (Section 3.3)
- Evaluation metric used in the uncertainty estimation (Section 4.1)
- Qualitative result for uncertainty maps on KITTI dataset (Section 4.2)

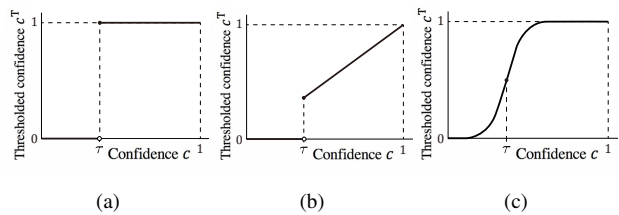


Figure 1. Comparison of confidence thresholding operator: (a) hard-thresholding used in [1], (b) hard-thresholding function used in [20], and (c) our soft-thresholding function. The learned threshold is used in (b) and (c), while the threshold is fixed in (a) for all training images.

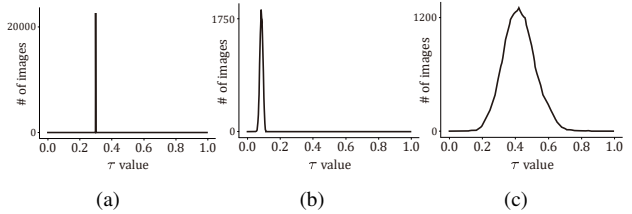


Figure 2. Histogram of the learned threshold τ on three different thresholding methods: (a) hard-thresholding used in [1], (b) hard-thresholding function used in [20], and (c) our soft-thresholding function.

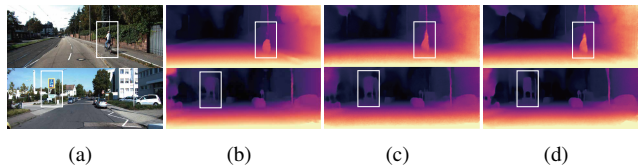


Figure 3. Examples of gradually improved depth results of (a) input image, from (b) using the monocular depth network with fixed threshold $\tau = 0.3$ [1], (c) using the monocular depth network with learned threshold τ [20], and to (d) using the proposed method.

1. Comparison with thresholding methods

This section further highlights the effectiveness of our thresholding method by analyzing the distribution of learned threshold τ . Fig. 1 recaps the thresholding oper-

* Equal contribution. † Corresponding author.

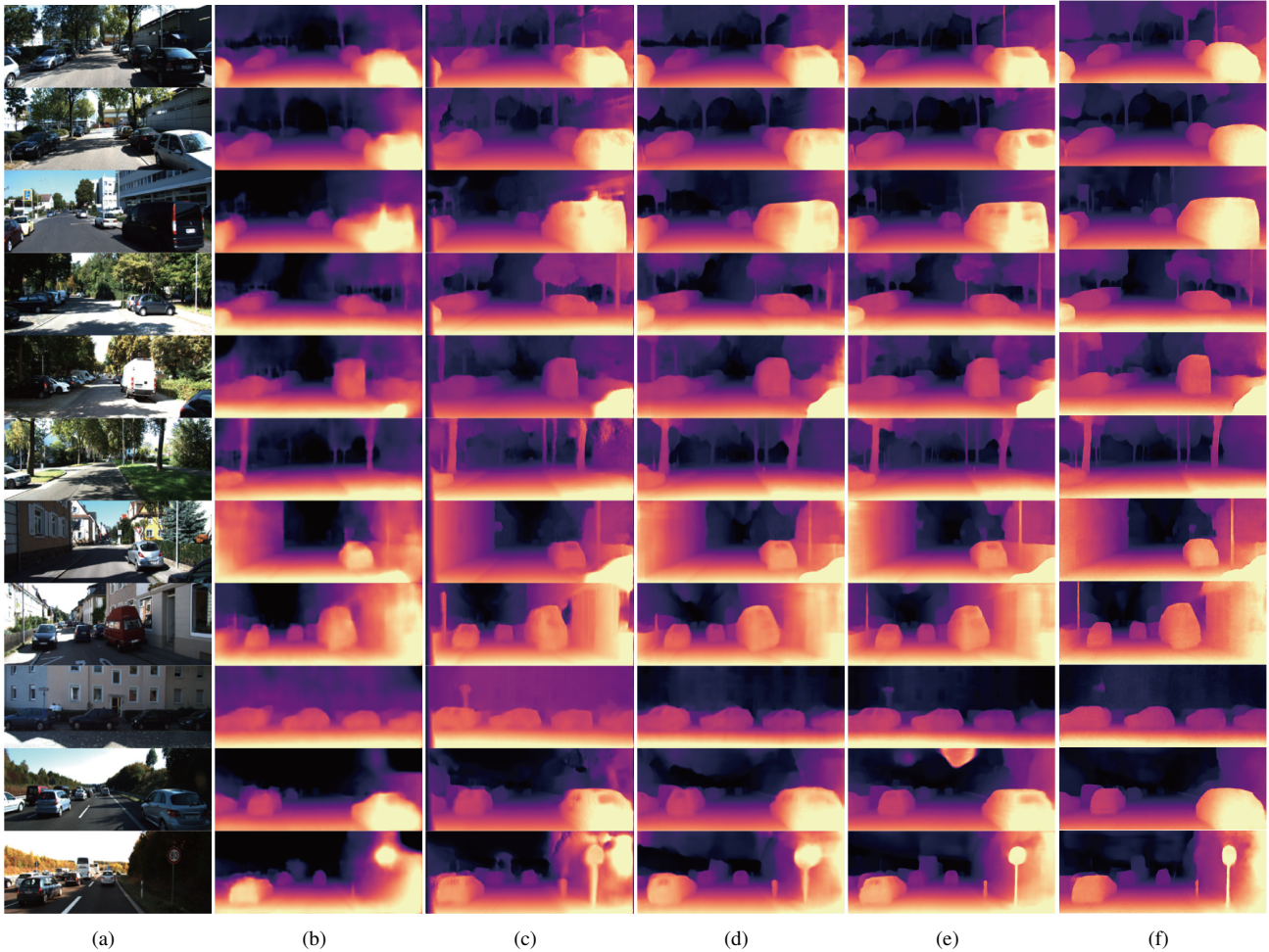


Figure 4. Qualitative evaluation with existing monocular depth estimation methods on the Eigen split [3] of KITTI dataset: (a) input image, (b) Kuznetsov *et al.* [13], (c) Monodepth [5], (d) Monodepth2 [6], (e) DepthHint [24], and (f) Ours (D+R) in the submitted manuscript. Compared to other results, our method predicts instances very well without holes or distortions while recovering fine object boundaries. Additionally, our method is capable of predicting thin instances precisely.

ators (Fig. 2 of the paper) for the completeness of supplementary document. To analyze the distribution of the learned threshold τ , we plotted the histogram of τ values learned using 20k images of KITTI training dataset [4] in Fig. 2. For a fair comparison, all experiments were conducted under the same environment, including network architecture, loss function, and training data. All results were obtained without the probabilistic refinement of the RefineNet.

Cho *et al.* [1] fixed the threshold to 0.3 for all training images. Tonioni *et al.* [20] attempted to learn the threshold adaptively for each image by applying the regularization loss $-\log(1 - \tau)$, but it simply prevents τ values from converging to 0 or 1 and does not take into account image characteristics that enable τ to be learned adaptively. As shown in Fig. 2 (b), τ values predicted by [20] are concentrated around specific values (0.1) with very small variance,

meaning that almost similar threshold τ is used for all training images. This is the reason why the performance gain of Tonioni *et al.* [20] over Cho *et al.* [1] is relatively marginal, as reported in Tab. 4 of the original manuscript. Contrarily, our method learns image-adaptive τ values as plotted in Fig. 2 (c). Fig. 3 of the original manuscript also reports that the proposed method learned the threshold τ accordingly. The threshold τ was set low in the images where depth inference is easy, while being set high in the opposite case including saturation, low-light, and textureless region.

Fig. 3 shows the examples of gradually improved depth results according to different thresholding methods. The proposed method yields qualitatively better results, where complete instances are recovered and fine object boundaries are well preserved, than other hard thresholding methods. Also, in Tab. 4 of the original manuscript, it can be seen that the proposed method outperforms the two methods quanti-

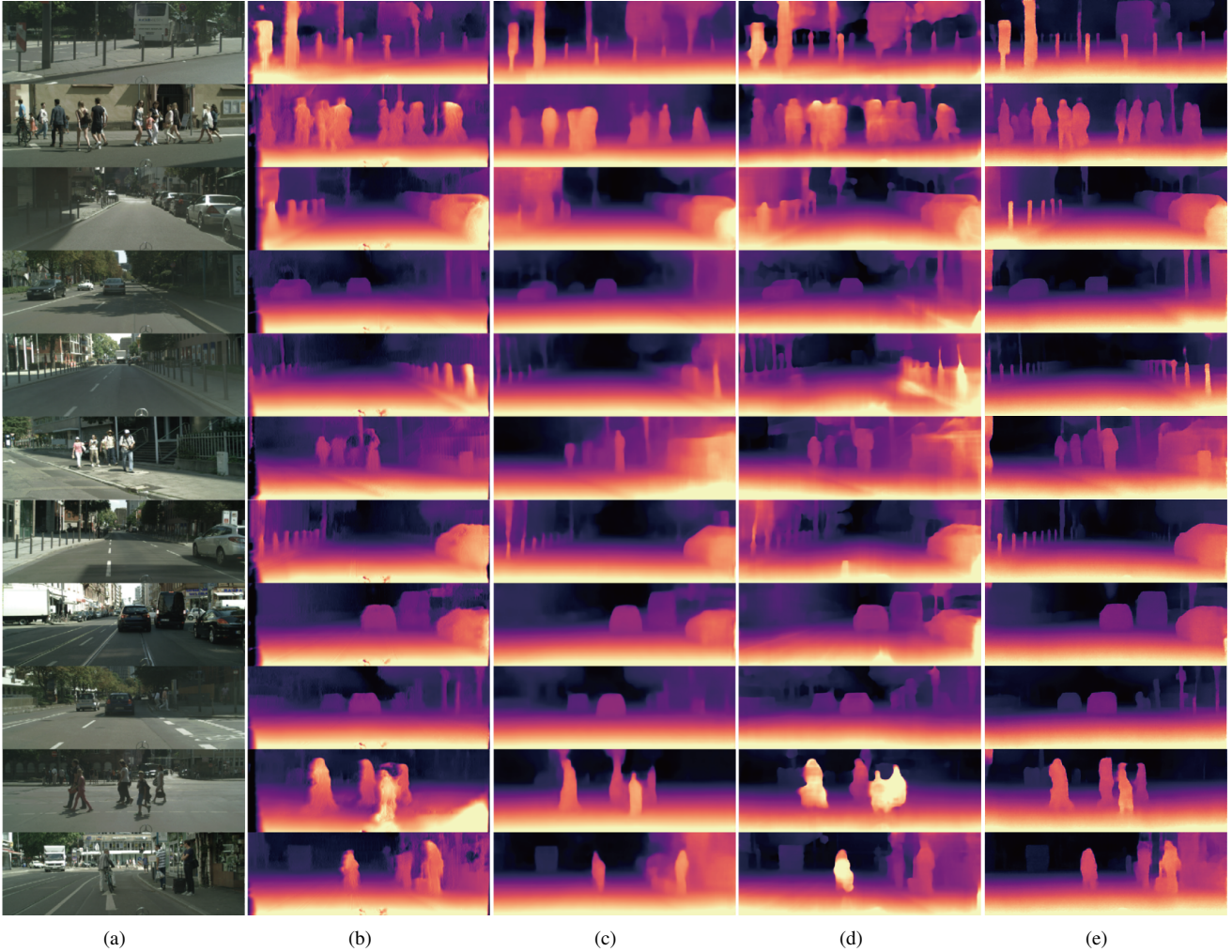


Figure 5. Qualitative evaluation for depth estimation with existing methods on Cityscapes validation dataset: (a) input image, (b) [5], (c) [21], (d) [24] and (e) Ours (D+R) of the original manuscript. Similar to KITTI results, our method is remarkable at predicting fine details with no distortions at all instances and recovering thin objects that appear frequently in the Cityscapes dataset, whereas other methods often fail to predict accurate depth values at these regions.

tatively.

2. Monocular depth estimation results

This section provides more results for comparative study with state-of-the-art methods in terms of monocular depth accuracy.

2.1. Evaluation metrics

In order to evaluate the depth estimation performance, same as the original manuscript, five commonly-used evaluation metrics proposed in [3] were adopted as follows:

- Abs Rel = $\frac{1}{|\Omega|} \sum_{p \in \Omega} \frac{|d_p - d_p^{\text{gt}}|}{d_p^{\text{gt}}}$
- Sq Rel = $\frac{1}{|\Omega|} \sum_{p \in \Omega} \frac{(d_p - d_p^{\text{gt}})^2}{d_p^{\text{gt}^2}}$

- RMSE = $\sqrt{\frac{1}{|\Omega|} \sum_{p \in \Omega} (d_p - d_p^{\text{gt}})^2}$

- RMSE log = $\sqrt{\frac{1}{|\Omega|} \sum_{p \in \Omega} (\log(d_p) - \log(d_p^{\text{gt}}))^2}$

- $\delta < 1.25^n = \% \text{ of } d_p \text{ s.t. } \delta = \max\left(\frac{d_p}{d_p^{\text{gt}}}, \frac{d_p^{\text{gt}}}{d_p}\right) < 1.25^n$
for $n = 1, 2, 3$,

where d_p and d_p^{gt} indicate the estimated depth map and ground truth depth map at a pixel p , respectively. Ω represents a set of valid pixels.

2.2. Qualitative evaluation on KITTI

Fig. 4 shows more results on the Eigen Split [3] of KITTI dataset. We compared our results with (b) Kuznetsov *et*

Table 1. Quantitative evaluation for depth estimation with existing methods on Cityscapes validation dataset without fine-tuning on Cityscapes training dataset. Numbers in bold and underlined represent 1st and 2nd ranking, respectively.

Method	Data	Lower is better				Accuracy: higher is better		
		Abs Rel	Sqr Rel	RMSE	RMSE log	$\delta < 1.25$	$\delta < 1.25^2$	$\delta < 1.25^3$
Monodepth [5]	S	0.631	10.257	13.424	0.525	0.281	0.546	0.749
MonoResMatch [21]	S	0.241	2.149	9.064	0.296	0.570	0.891	0.966
PackNet-SfM [7]	M	0.245	2.240	8.920	0.298	0.557	0.892	0.967
Monodepth2 [6]	S	0.242	2.308	8.563	0.290	0.591	0.904	0.971
DepthHint [24]	S	0.220	2.008	8.363	0.273	0.613	0.922	<u>0.975</u>
Ours (D)	S	0.238	<u>1.983</u>	<u>8.176</u>	0.282	<u>0.629</u>	<u>0.923</u>	0.976
Ours (D+R)	S	<u>0.225</u>	1.962	8.010	<u>0.276</u>	0.631	0.924	0.976

Table 2. Quantitative evaluation for monocular depth estimation with existing methods on KITTI Eigen split dataset [3] with improved ground truth depth maps [22]. Numbers in bold and underlined represent 1st and 2nd ranking, respectively.

Method	Data	Lower is better				Accuracy: higher is better		
		Abs Rel	Sqr Rel	RMSE	RMSE log	$\delta < 1.25$	$\delta < 1.25^2$	$\delta < 1.25^3$
SfMLearner [25]	M	0.176	1.532	6.129	0.244	0.758	0.921	0.971
Vid2Depth [15]	M	0.134	0.983	5.501	0.203	0.827	0.944	0.981
DDVO [23]	M	0.126	0.866	4.932	0.185	0.851	0.958	0.986
EPC++ [14]	M	0.120	0.789	4.755	0.177	0.856	0.961	0.987
Monodepth2 [6]	S	0.090	0.545	3.942	0.137	0.914	0.983	<u>0.995</u>
Uncertainty (Boot+Log) [17]	S	0.085	0.511	3.777	0.137	0.913	0.980	0.994
Uncertainty (Boot+Self) [17]	S	0.085	0.510	3.792	0.135	0.914	0.981	0.994
Uncertainty (Snap+Log) [17]	S	0.084	0.529	3.833	0.138	0.914	0.980	0.994
Uncertainty (Snap+Self) [17]	S	0.086	0.532	3.858	0.138	0.912	0.980	0.994
UnRectDepthNet [12]	M	0.081	0.414	3.412	0.117	0.926	0.987	0.996
PackNet-SfM [7]	M	<u>0.078</u>	0.420	3.485	0.121	0.931	<u>0.986</u>	0.996
Ours (D)	S	<u>0.078</u>	<u>0.361</u>	<u>3.223</u>	0.120	<u>0.930</u>	0.987	0.996
Ours (D+R)	S	0.076	0.340	3.171	<u>0.119</u>	0.931	0.987	0.996

al. [13], (c) Monodepth [5], (d) Monodepth2 [6], (e) DepthHint [24], and (f) Ours (D+R). Compared to other results, our method predicts instances very well without holes or distortions while recovering fine object boundaries. Additionally, our method is capable of predicting thin objects precisely.

2.3. Qualitative evaluation on Cityscapes dataset

Fig. 5 shows more qualitative results on Cityscapes dataset [2] of Fig. 5 in original manuscript. Note that it is fine-tuned on Cityscapes dataset. We compared our results with three existing methods: (b) [5], (c) [21], (d) [24] and (e) Ours (D+R) in the original manuscript. Similar to KITTI results, our method is remarkable at predicting fine details with no distortions at all instances and recovering thin objects that appear frequently in the Cityscapes dataset, whereas other methods often fail to predict accurate depth values at these regions.

2.4. Quantitative evaluation on Cityscapes dataset without fine-tuning

We also evaluated the performance of the proposed method on the Cityscapes dataset without fine-tuning. Table 1 provides the quantitative evaluation on the Cityscapes validation dataset [2], setting maximum depth to 80 meters. The performance evaluation includes Monodepth [5], MonoResMatch [21], Monodepth2 [6], DepthHint [24], PackNet-SfM [7]. Even without fine-tuning on the Cityscapes dataset, our method still outperforms state-of-the-arts approaches, and it shows that our model trained on KITTI dataset generalizes well on other dataset without bias.

2.5. Quantitative evaluation on KITTI improved ground truth depth maps

To strengthen credibility to quantitative evaluation, we also measured the monocular depth accuracy by using test frames with the improved ground truth depth maps made available in [22] for KITTI Eigen split dataset [3]. The improved ground truth maps are high quality depth maps gen-

Table 3. Quantitative depth estimation results according to ε value evaluated on KITTI Eigen Split [3] raw dataset.

ε	Abs Rel	Sqr Rel	RMSE	RMSE log	$\delta < 1.25$	$\delta < 1.25^2$	$\delta < 1.25^3$
10	0.099	0.652	4.266	0.187	0.883	0.960	0.981
30	0.102	0.657	4.290	0.189	0.881	0.959	0.980
50	0.100	0.649	4.272	0.188	0.881	0.959	0.979

Table 4. Quantitative depth estimation results for three cases of the proposed method on KITTI Eigen Split [3] raw dataset.

Method	Abs Rel	Sqr Rel	RMSE	RMSE log	$\delta < 1.25$	$\delta < 1.25^2$	$\delta < 1.25^3$
Ours (D)	0.099	0.652	4.266	0.187	0.883	0.960	0.981
Ours (R)	0.096	0.646	4.280	0.189	0.882	0.959	0.980
Ours (D+R)	0.096	0.629	4.187	0.185	0.887	0.963	0.983

erated by accumulating LiDAR point clouds from 5 consecutive frames. Table 2 shows the quantitative evaluation with existing methods on the KITTI Eigen split dataset using the improved ground truth depth maps [22]. We compared our results with ‘SfMLeaer’ [25], ‘Vid2Depth’ [15], ‘DDVO’ [23], ‘EPC++’ [14], ‘Monodepth2’ [6], ‘Uncertainty’ [17], ‘PackNet-SfM’ [7], and ‘UnRectDepthNet’ [12]. For the training data, ‘M’ and ‘S’ indicate using a monocular video sequence and stereo images, respectively. Our method produces superior performance compared to other methods.

2.6. Choice of ε value

We set $\varepsilon = 10$ for the differentiable soft-thresholding function in (1) of the original manuscript. Table 3 shows the quantitative results according to ε on the KITTI Eigen split [3] raw dataset. Though the best accuracy was achieved with $\varepsilon = 10$, no significant change was observed depending on varying ε .

2.7. Ablation study of DepthNet and RefineNet

The evaluation of the proposed method was conducted for three cases; ‘Ours (D)’ trained with only the DepthNet using L_D without refining the depth map, ‘Ours (R)’ trained with the DepthNet and RefineNet using L_U only, and ‘Ours (D+R)’ trained with the DepthNet and RefineNet using all losses. Table 4 shows the quantitative results of the above three cases on KITTI Eigen Split [3] dataset. The performance gain of ‘Ours (D+R)’ over ‘Ours (R)’ supports the effectiveness of the proposed confidence learning.

3. Confidence estimation results

3.1. Generating ground-truth confidence map

To train the confidence network, the ground truth confidence map is required as supervision. Following existing confidence estimation approaches [18, 11], the ground truth confidence map c_p^{gt} was computed by using an absolute difference between the ground truth disparity map and the input disparity map (the pseudo ground truth disparity map in

our work).

$$c_p^{\text{gt}} = \begin{cases} 1, & \text{if } |d_p - d_p^{\text{gt}}| \leq \rho. \\ 0, & \text{otherwise.} \end{cases} \quad (1)$$

The threshold value ρ is set to 3 for KITTI [16] and 1 for Middlebury [19].

3.2. Evaluation metric

The area under the curve (AUC) [9] was used for evaluating the performance of estimated confidence maps. The receiver operating characteristic (ROC) curve is first computed by sorting disparity pixels in a decreasing order of confidence and sequentially sampling high confidence disparity pixels. It computes the error rate indicating the percentage of pixels with a difference larger than ρ from ground truth disparity. Then, AUC is computed by integral of the ROC curve. The optimal AUC is computed according to the fact that the error rate ζ is ideally 0 when sampling the first $(1 - \zeta)$ pixels [9], which is equal to

$$AUC_{opt} = \int_{1-\zeta}^1 \frac{x - (1 - \zeta)}{x} dx = \zeta + (1 - \zeta) \ln 1 - \zeta. \quad (2)$$

3.3. Qualitative evaluation on KITTI 2015 dataset

Fig. 6 shows more qualitative results of confidence map evaluated on KITTI 2015 dataset [16]. Input disparity maps used for confidence estimation were obtained by Census-SGM [8]. The estimated confidence maps for each input disparity map are displayed every two rows. The top and bottom of two rows indicate: (a) color image and input disparity image, (b) CCNN [18] and CCNN w/ τ , (c) LAFNet* [11] and LAFNet* w/ τ and (d) LAFNet and LAFNet w/ τ . ‘w/ τ ’ denotes the thresholded confidence map obtained using the soft-thresholding. LAFNet* denotes the LAFNet [11] in which 3D cost volume is not used as an input. As shown in Fig. 6, the proposed thresholded confidence maps contain fewer ambiguous values than the original confidence maps.

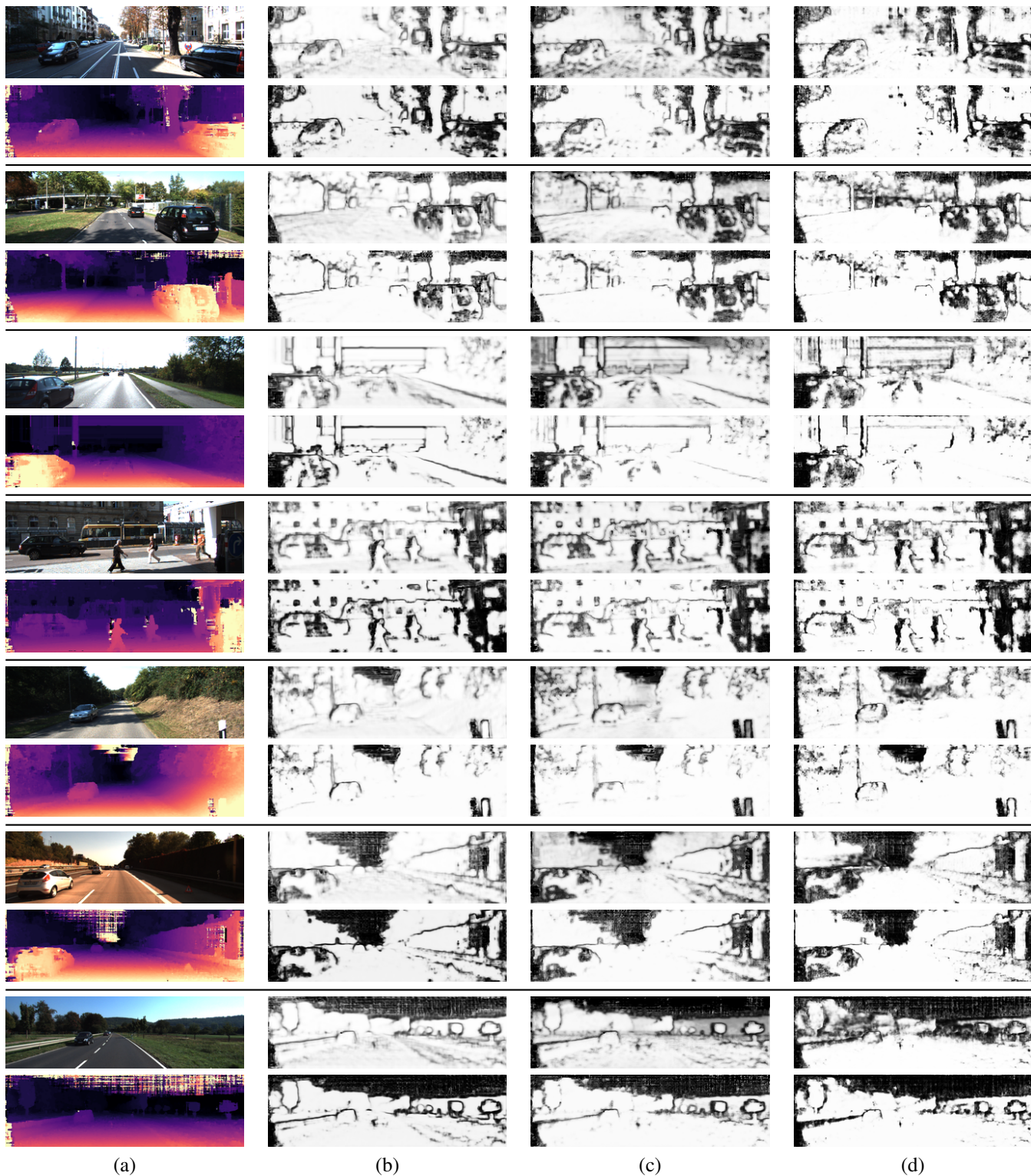


Figure 6. Qualitative evaluation for confidence estimation on KITTI 2015 dataset [16]: Input disparity maps used for confidence estimation were obtained by Census-SGM [8]. The estimated confidence maps for each input disparity map are displayed every two rows. The top and bottom of two rows indicate: (a) color image and input disparity image, (b) CCNN [18] and CCNN w/τ , (c) LAFNet* [11] and LAFNet* w/τ and (d) LAFNet and LAFNet w/τ . ‘ w/τ ’ denotes the proposed network using the soft-thresholding. LAFNet* denotes the LAFNet [11] in which 3D cost volume is not used as an input.

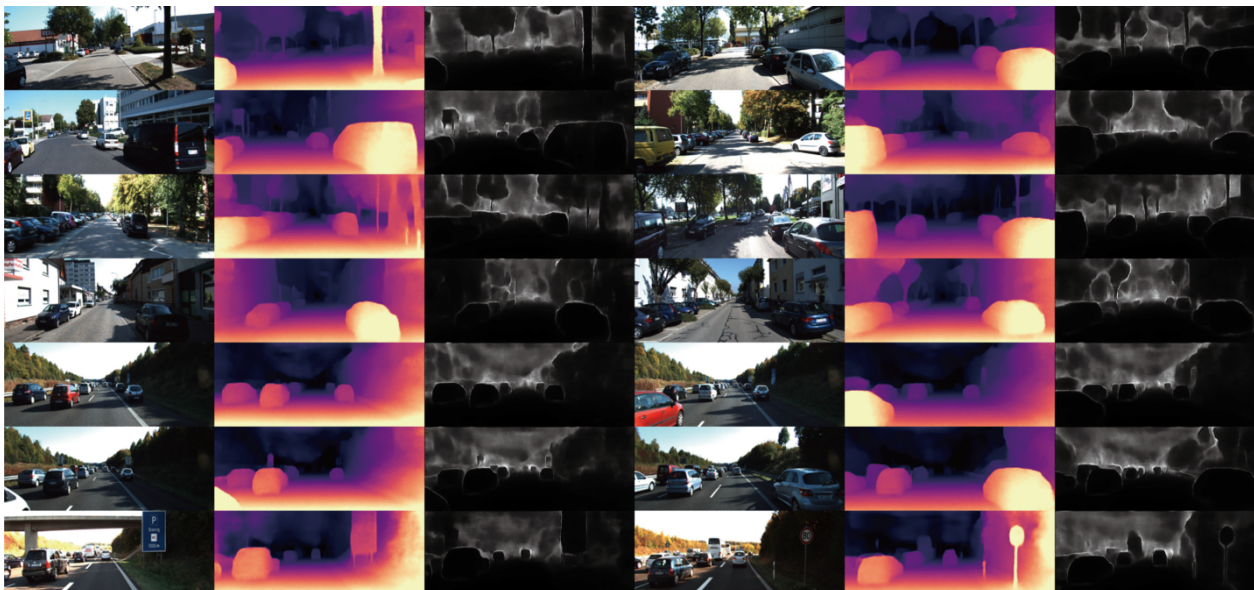


Figure 7. Qualitative result of uncertainty measure on KITTI Eigen Split [3] test dataset. From left to right, input image, estimated depth map, and uncertainty map of the estimated depth are displayed.

4. Uncertainty Estimation Details

4.1. Evaluation metric

We evaluated the performance of the uncertainty estimation used in the proposed model using the sparsification error [10]. Similar to the confidence evaluation, we first sorted disparity pixels following decreasing order of uncertainty, and iteratively extracted high uncertain disparities and provided them as inputs for computing error metrics. The ideal error ranked by the true error to the ground truth is referred to as oracle. With a sparsification error, we computed the Area Under the Sparsification Error curve (AUSE) and the Area Under the Random Gain (AURG) to evaluate the quality of the uncertainty map. While the AUSE is measured as the difference between the sparsification and its oracle, the AURG is obtained as subtracting the estimated sparsification curve from flat curve with a random uncertainty which is modeled as a constant.

4.2. Qualitative evaluation on KITTI dataset

Fig. 7 shows the qualitative results of uncertainty map evaluated on KITTI Eigen Split [3] test dataset. The qualitative result indicates that uncertain areas of the estimated depth map are usually located around object boundaries and sky.

References

[1] Jaehoon Cho, Dongbo Min, Youngjung Kim, and Kwanghoon Sohn. A large rgb-d dataset for semi-

- supervised monocular depth estimation. *arXiv preprint arXiv:1904.10230*, 2019. 1, 2
- [2] Marius Cordts, Mohamed Omran, Sebastian Ramos, Timo Rehfeld, Markus Enzweiler, Rodrigo Benenson, Uwe Franke, Stefan Roth, and Bernt Schiele. The cityscapes dataset for semantic urban scene understanding. In *Proceedings of the IEEE conference on computer vision and pattern recognition*, pages 3213–3223, 2016. 4
- [3] David Eigen, Christian Puhrsch, and Rob Fergus. Depth map prediction from a single image using a multi-scale deep network. In *Advances in neural information processing systems*, pages 2366–2374, 2014. 2, 3, 4, 5, 7
- [4] Andreas Geiger, Philip Lenz, Christoph Stiller, and Raquel Urtasun. Vision meets robotics: The kitti dataset. *The International Journal of Robotics Research*, 32(11):1231–1237, 2013. 2
- [5] Clément Godard, Oisín Mac Aodha, and Gabriel J Brostow. Unsupervised monocular depth estimation with left-right consistency. In *Proceedings of the IEEE Conference on Computer Vision and Pattern Recognition*, pages 270–279, 2017. 2, 3, 4
- [6] Clément Godard, Oisín Mac Aodha, Michael Firman, and Gabriel J Brostow. Digging into self-supervised monocular depth estimation. In *Proceedings of the IEEE international conference on computer vision*, pages 3828–3838, 2019. 2, 4, 5
- [7] Vitor Guizilini, Rares Ambrus, Sudeep Pillai, Allan Raventos, and Adrien Gaidon. 3d packing for self-supervised monocular depth estimation. In *Proceedings of the IEEE/CVF Conference on Computer Vision and Pattern Recognition*, pages 2485–2494, 2020. 4, 5
- [8] Heiko Hirschmüller. Accurate and efficient stereo processing by semi-global matching and mutual information. In *2005 IEEE Computer Society Conference on Computer Vision and*

- Pattern Recognition (CVPR'05)*, volume 2, pages 807–814. IEEE, 2005. 5, 6
- [9] Xiaoyan Hu and Philippos Mordohai. A quantitative evaluation of confidence measures for stereo vision. *IEEE transactions on pattern analysis and machine intelligence*, 34(11):2121–2133, 2012. 5
- [10] Eddy Ilg, Ozgun Cicek, Silvio Galesso, Aaron Klein, Osama Makansi, Frank Hutter, and Thomas Brox. Uncertainty estimates and multi-hypotheses networks for optical flow. In *Proceedings of the European Conference on Computer Vision (ECCV)*, pages 652–667, 2018. 7
- [11] Sunok Kim, Seungryong Kim, Dongbo Min, and Kwanghoon Sohn. Laf-net: Locally adaptive fusion networks for stereo confidence estimation. In *Proceedings of the IEEE Conference on Computer Vision and Pattern Recognition*, pages 205–214, 2019. 5, 6
- [12] Varun Ravi Kumar, Senthil Yogamani, Markus Bach, Christian Witt, Stefan Milz, and Patrick Mader. Unrectdepthnet: Self-supervised monocular depth estimation using a generic framework for handling common camera distortion models. *arXiv preprint arXiv:2007.06676*, 2020. 4, 5
- [13] Yevhen Kuznietsov, Jorg Stuckler, and Bastian Leibe. Semi-supervised deep learning for monocular depth map prediction. In *Proceedings of the IEEE conference on computer vision and pattern recognition*, pages 6647–6655, 2017. 2, 4
- [14] Chenxu Luo, Zhenheng Yang, Peng Wang, Yang Wang, Wei Xu, Ramkant Nevatia, and Alan Yuille. Every pixel counts++: Joint learning of geometry and motion with 3d holistic understanding. *IEEE transactions on pattern analysis and machine intelligence*, 2019. 4, 5
- [15] Reza Mahjourian, Martin Wicke, and Anelia Angelova. Unsupervised learning of depth and ego-motion from monocular video using 3d geometric constraints. In *Proceedings of the IEEE Conference on Computer Vision and Pattern Recognition*, pages 5667–5675, 2018. 4, 5
- [16] Moritz Menze and Andreas Geiger. Object scene flow for autonomous vehicles. In *Proceedings of the IEEE conference on computer vision and pattern recognition*, pages 3061–3070, 2015. 5, 6
- [17] Matteo Poggi, Filippo Aleotti, Fabio Tosi, and Stefano Mattoccia. On the uncertainty of self-supervised monocular depth estimation. In *Proceedings of the IEEE/CVF Conference on Computer Vision and Pattern Recognition*, pages 3227–3237, 2020. 4, 5
- [18] Matteo Poggi and Stefano Mattoccia. Learning from scratch a confidence measure. In *BMVC*, 2016. 5, 6
- [19] Daniel Scharstein, Heiko Hirschmüller, York Kitajima, Greg Krathwohl, Nera Nešić, Xi Wang, and Porter Westling. High-resolution stereo datasets with subpixel-accurate ground truth. In *German conference on pattern recognition*, pages 31–42. Springer, 2014. 5
- [20] Alessio Tonioni, Matteo Poggi, Stefano Mattoccia, and Luigi Di Stefano. Unsupervised domain adaptation for depth prediction from images. *IEEE transactions on pattern analysis and machine intelligence*, 2019. 1, 2
- [21] Fabio Tosi, Filippo Aleotti, Matteo Poggi, and Stefano Mattoccia. Learning monocular depth estimation infusing traditional stereo knowledge. In *Proceedings of the IEEE Conference on Computer Vision and Pattern Recognition*, pages 9799–9809, 2019. 3, 4
- [22] Jonas Uhrig, Nick Schneider, Lukas Schneider, Uwe Franke, Thomas Brox, and Andreas Geiger. Sparsity invariant cnns. In *2017 international conference on 3D Vision (3DV)*, pages 11–20. IEEE, 2017. 1, 4, 5
- [23] Chaoyang Wang, José Miguel Buenaposada, Rui Zhu, and Simon Lucey. Learning depth from monocular videos using direct methods. In *Proceedings of the IEEE Conference on Computer Vision and Pattern Recognition*, pages 2022–2030, 2018. 4, 5
- [24] Jamie Watson, Michael Firman, Gabriel J Brostow, and Daniyar Turmukhambetov. Self-supervised monocular depth hints. In *Proceedings of the IEEE International Conference on Computer Vision*, pages 2162–2171, 2019. 2, 3, 4
- [25] Tinghui Zhou, Matthew Brown, Noah Snavely, and David G Lowe. Unsupervised learning of depth and ego-motion from video. In *Proceedings of the IEEE Conference on Computer Vision and Pattern Recognition*, pages 1851–1858, 2017. 4, 5